

## Optical impacts of oceanic coccolithophore blooms

T. Tyrrell and P. M. Holligan

School of Ocean and Earth Science, Southampton Oceanography Centre, University of Southampton, Southampton, United Kingdom

C. D. Mobley

Sequoia Scientific Inc., Mercer Island, Washington

**Abstract.** Blooms of coccolithophores, particularly those of the species *Emiliania huxleyi*, cause light in the surface ocean to behave in an unusual fashion, producing distinctive bright “white waters,” apparent from ships and readily detected by remote sensing. The brightness is caused by scattering of light from calcium carbonate platelets (coccoliths). Here we present the results of a modeling study, giving precise calculations of how the coccolith light scattering changes the behavior of light in the water. The results from a Monte Carlo optical model are closely compared to data from the CD60 cruise for a coccolithophore bloom south of Iceland in 1991 [Holligan *et al.*, 1993], and the model is then used to extrapolate from the observational data to predict diverse optical properties that were not measured. Model performance was also tested by comparison of results with those from other, more established optical models. The model results demonstrate clearly that coccoliths cause (1) an increase in the emergent flux (the water-leaving radiance), (2) brighter, more intensely heated water in the top few meters, and (3) darker, less intensely heated water deeper down. Implications of these effects for phytoplankton productivity and for climatology are discussed. Coccolith light scattering is estimated to contribute to global annually averaged planetary albedo by a maximum of  $\sim 0.13\%$ , equivalent to only a small globally averaged radiative forcing of  $\sim 0.22 \text{ W m}^{-2}$ .

### 1. Introduction

Coccolithophores are phytoplankton which synthesize minute calcium carbonate platelets (coccoliths) around the surface of their cells. Coccolithophores are widespread in all oceans except the polar ones [Winter *et al.*, 1994]. However, bloom proportions ( $> 1000 \text{ cells mL}^{-1}$ ) are only attained in a few areas, most notably the subarctic North Atlantic and adjacent seas [Brown and Yoder, 1994], and are usually attributable to a single species, *Emiliania huxleyi*. As far as we know, *E. huxleyi* is unique among the coccolithophores, in that coccoliths from the cell surface are shed in large numbers into the surrounding water. During blooms of this species (up to  $100,000 \text{ km}^2$  or more in extent [Brown and Yoder, 1994]), large numbers of cells (e.g.,  $10,000 \text{ cells mL}^{-1}$  [Holligan *et al.*, 1993]) are usually accompanied by much larger numbers of detached coccoliths (e.g.,  $300,000 \text{ coccoliths mL}^{-1}$  [Holligan *et al.*, 1993]) suspended in the water. The coccoliths scatter but do not absorb light, acting somewhat like tiny mirrors dis-

persed in the water. The resulting “white waters” of these blooms have frequently been remarked upon by mariners, and the perturbation of the light coming back out of the ocean makes these blooms easily detectable from space.

It is known that the coccoliths cause unusual optical behavior [Holligan and Balch, 1991], but the exact effects have not yet been determined. What are the implications for stratification, productivity, and climatology of these dense blooms which periodically blanket the northeast Atlantic? In this paper a sophisticated multispectral, multicomponent Monte Carlo optical model is used to gain a qualitative and quantitative understanding of the nature and implications of coccolith effects on surface layer optics.

There are two aspects to a model investigation of this sort. The first step is to build the model in such a way that all the processes are modeled correctly. That is to say, the frequency of absorption and scattering events are both represented accurately, the proportion of scattering events that are at small angles and at large angles are in accordance with the scattering phase function, interactions at the air-sea interface agree with experiment and theory, and other processes are properly characterized. This first step creates a generic framework allow-

Copyright 1999 by the American Geophysical Union.

Paper number 1998JC900052.  
0148-0227/99/1998JC900052\$09.00

ing light behavior in almost any type of water to be simulated. The second step is to obtain measurements, or to derive estimates, of the specific water conditions under which the model is to be run. The inherent optical properties (IOPs) of the water must be specified, and, in addition, the incident radiant flux (the skylight plus the direct sunlight) must be parameterized. When the incident radiation and the water body are both accurately represented in the model, the simulation can then run its course for a particular situation and generate predictions of resulting irradiances, reflectances, attenuations, heating rates, photon budgets, etc. In this paper the construction of the model is described, followed by the specification of IOPs and incident radiation and finally the model outputs.

This work builds upon previous work on (1) the relationship between coccolith concentration and the intensity of photon scattering, and (2) the shape of the scattering phase function for coccoliths [Balch *et al.*, 1991, 1996a,b]. These results have allowed estimation of the effects of coccoliths on the IOPs, which is an essential precursor to the calculation here of the effects on the full radiance distribution and derived optical variables.

## 2. Model Description

A multispectral, multicomponent Monte Carlo model, henceforth referred to as the Coccolithophore Optics (COPT) model, was constructed in order to examine coccolith optical impacts. It is a simulation of the behavior of thousands or millions of photons arriving at the sea surface and subsequently interacting probabilistically with the surface and (for those that are not reflected) with the water. By averaging over the large population of photons, an estimate of the bulk light field is obtained. This model is based on Kirk's [1981] simple multispectral Monte Carlo model but has been improved in several ways. The equations have been modified to calculate azimuth as well as zenith angles of photons in the water (making it three dimensional (3-D) rather than just two-dimensional (2-D)), and more components (including coccoliths) have been added to the factors affecting the absorption coefficient and the scattering coefficient.

### 2.1. Direct and Diffuse Incident Irradiance

Incident irradiance has also been changed from Kirk's [1981] basic model, from a simple point source representing the sun to a full representation of the skylight (diffuse light) in addition to the direct solar beam. This has been implemented exactly according to the formula of Harrison and Coombes [1988], which takes account of sun zenith angle and cloud cover to calculate the full 3-D radiance distribution of the light arriving from the atmosphere. An example radiance distribution for the downwelling incident light impinging on the water surface is shown in Figure 1 for a zenith angle of 45° and 25% cloudiness.

### 2.2. Air-Sea Interface

Kirk's [1981] basic model was also extended by the inclusion of a wind-roughened sea surface, to replace the original flat sea surface. This was achieved by generating wave facets with slopes chosen probabilistically from a distribution dependent on the wind speed, but not dependent on the wind direction, according to the formula [Cox and Munk, 1954]

$$\sigma^2 = 0.003 + 0.00512 \times U \quad (1)$$

where  $\sigma$  is the standard deviation of the normal distribution of wave slopes (mean 0.0) and  $U$  is the wind speed ( $\text{m s}^{-1}$ ). This formula, together with consideration of the "apparent area" of a facet when looking along the line of travel of a particular photon (for instance, a facet whose normal is perpendicular to the incoming photon has no chance of intercepting it), was used to generate probabilities of photons at different orientations impinging on wave facets at different orientations. Once a photon was matched to a wave facet using a random number, Fresnel's equation was then applied to calculate the probability of reflection of the photon from the wave facet.

The resulting reflection probabilities (averaging over many photons) for photons traveling from air to sea and from sea to air, for a range of different angles to the vertical, are shown in Figure 2 for a wind speed of 5  $\text{m s}^{-1}$ . These graphs and the wind speed dependence of surface reflection in the COPT model (not shown) are in reasonable agreement with the expected probabilities [Kirk, 1994, Figure 2.10; Mobley, 1994, Figures 4.12, 4.15].

One aspect of the original model that was not modified is the assumption that the IOPs are constant with depth in the mixed layer. In COPT the mixed layer is vertically homogeneous, overlying a deeper layer in which the only attenuation is that due to water. This is a simplification of the real-life conditions, as shown for example in Figure 6.

### 2.3. Comparisons

The adequacy of the COPT model was checked by comparing different 3-D radiance distributions produced by the model. For instance, the above-surface incident downward radiance was compared to the same flux after transmission down through the sea surface, and the focusing of the solar beam and the shift toward the vertical (due to refraction) were both observed (Figure 3; to be compared to Figure 1).

The results of several established optical models (both Monte Carlo and analytical) have been compared for some canonical test situations [Mobley *et al.*, 1993]. The performance of the COPT model was also examined for the same test situations. To carry out the comparison, depth profiles of  $E_d$ ,  $E_{ou}$  (upwelling scalar irradiance), and  $L_u$  (radiance intensity in the upward vertical direc-

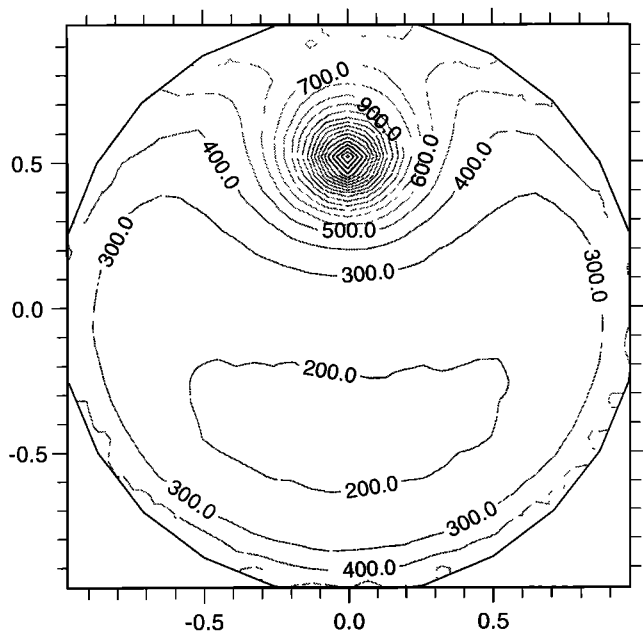


**Figure 1.** Downward radiance (sum of direct solar beam + diffuse skylight) incident on water surface, calculated in the COPT model according to the algorithm of *Harrison and Coombes* [1988] for a solar zenith angle of  $45^\circ$  and cloudiness of 25%. The flat visualization of hemispherical radiance is produced by mapping the zenith ( $\theta$ ) and azimuthal ( $\phi$ ) angles onto ( $r, \alpha$ ) using  $r = \theta/90^\circ$  and  $\alpha = \phi$ , where  $r$  and  $\alpha$  are distance from center and azimuth angle in two dimensions.

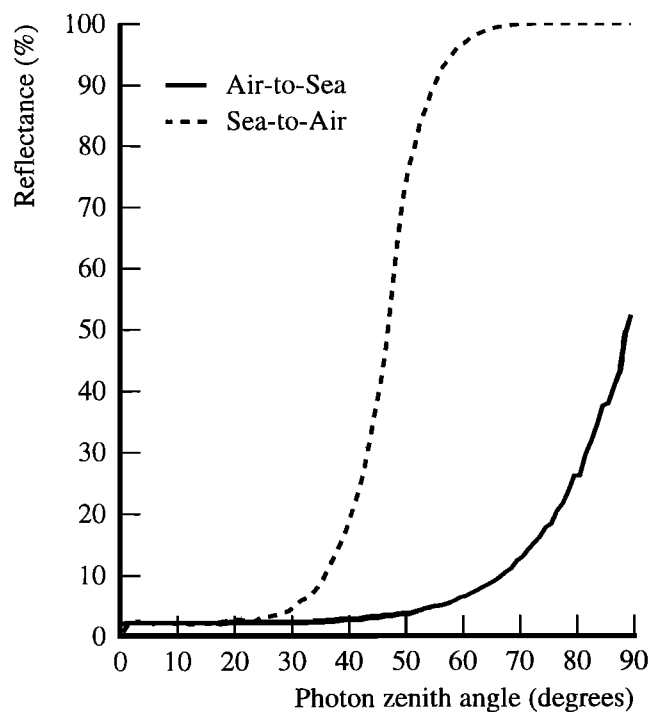


**Figure 2.** COPT model sea surface reflectance (percent) as a function of photon zenith angle (degrees) for photons traveling downward in the atmosphere toward the water (solid line) and upward in water toward the atmosphere (dashed line). Wind speed is  $5 \text{ m s}^{-1}$ .

tion) were generated for the specified water and solar conditions and compared to the results described for the other models. COPT results were only compared for problems 1, 2a ( $\omega_0 = 0.9$ ), 2b ( $\omega_0 = 0.2$ ), and 5 of the paper because other tests examined stratified water, atmospheric effects, a finite-depth bottom, or Raman scattering, none of which are included in COPT. For the comparisons that were made, COPT gives  $E_d$ ,  $E_{0u}$ , and  $L_u$  results which are close to (nearly all within 5%, maximum difference of 12%) the consensus solutions [Mobley *et al.*, 1993, Table 5]. Finally, the COPT results and those from the HYDROLIGHT invariant imbedded model [Mobley, 1995] were compared for several water cases (varied amounts of chlorophyll and coccoliths), and the solutions agreed to within 6% on each occasion.

### 3. Inherent Optical Properties

There are two aspects to specifying the IOPs: First, the model has to be set up to cause water and various particles or substances in the water to absorb and scatter photons appropriately; second, the concentrations and impacts of the various components have to be specified for the particular situation being modeled (in this case, the northeast Atlantic at  $\sim 60^\circ\text{N}$ ,  $20^\circ\text{W}$ , in June 1991).

#### 3.1. Absorption

The scattering ( $b$ ) and absorption ( $a$ ) coefficients in the model are calculated by summing contributions from different components. The absorption coefficient  $a(\lambda)$  is calculated as the sum of absorption due to pure seawater  $a_w(\lambda)$ , due to chlorophyll and other photosynthetic pigments  $a_{chl}(\lambda)$ , due to gilvin  $a_g(\lambda)$ , and due to detritus  $a_d(\lambda)$ :

$$a(\lambda) = a_w(\lambda) + (\text{chl} \times a_{chl}(\lambda)) + a_g(\lambda) + a_d(\lambda) \quad (2)$$

where chl is the concentration of chlorophyll  $a$ .

The spectral variation in absorption by seawater is taken from *Smith and Baker* [1981] and that by  $1 \text{ mg m}^{-3}$  of chlorophyll  $a$  is taken from *Morel and Prieur* [1977]. The spectral variation in absorption due to gilvin (yellow substance) is represented as outlined by *Kirk* [1994, section 3.3], using the equation

$$a_g(\lambda) = a_g(440) \times e^{-0.014 \times (\lambda - 440)} \quad (3)$$

where 0.014 is an empirical constant [Kirk, 1994, p. 63] and  $a_g(440)$  is the absorption due to gilvin at 440 nm. Gilvin concentrations are generally low in open ocean waters, with typical  $a_g(440)$  values of between 0.0 and 0.10 [Kirk, 1994, Table 3.2]. Absorption due to gilvin was not measured during the CD60 cruise and so cannot be constrained by measurements. Various values of  $a_g(440)$  were tried in the COPT model, and the best fits of model results and data (section 4) were obtained

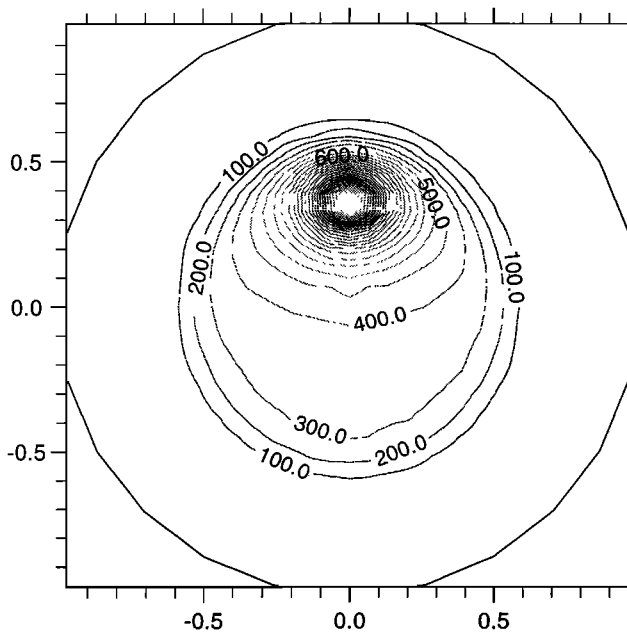


**Figure 3.** Surface-transmitted downward radiance; that is, the radiance that hits the water surface and is transmitted (refracted) by it, not reflected back up by it. The figure portrays this radiance just below the water surface, for the above-surface downwelling radiance of Figure 1.

with a value of  $a_g(440) = 0.075$ , which was then used throughout.

The spectral contribution of particulate detritus (tripton) to absorption was again not measured directly during CD60 but could be estimated from graphs of  $a_p(440)$  and  $a_p(550)$  versus chl  $a$  (W.M. Balch, unpublished data, 1997). At zero and near-zero values of chlorophyll, the values of particulate absorption  $a_p(\lambda)$  should represent the absorption due to detritus. In this case this analysis indicates that  $a_d(440) \simeq 0.020$  and  $a_d(550) \simeq 0.005$ . It is suggested [Roesler *et al.*, 1989] that the spectral variation in absorption due to detritus varies according to an equation of the form

$$a_d(\lambda) = a_d(400) \times e^{-0.011 \times (\lambda - 400)} \quad (4)$$

and this equation was used for  $a_d(\lambda)$  in the model;  $a_d(400)$  was given the value of 0.0285 in the model as a compromise between a curve intersecting  $a_d(440) = 0.020$  and a curve intersecting  $a_d(550) = 0.005$ . Figure 4a shows the contributions of each component to absorption in the COPT model, when there is 1 mg chl  $a$   $m^{-3}$  in the water.

### 3.2. Scattering

**3.2.1. Total scattering.** The scattering coefficient at each wavelength ( $b(\lambda)$ ) is similarly calculated as

$$b(\lambda) = b_w(\lambda) + (\text{CaCO}_3 \times b_{\text{CaCO}_3}(\lambda)) + b_p(\lambda) \quad (5)$$

where  $b_w(\lambda)$  is the small contribution due to pure seawater at each wavelength,  $b_p(\lambda)$  is the effect on scattering of noncalcite particulates (including chlorophyll),  $\text{CaCO}_3$  is the concentration of calcite ( $\text{mg CaCO}_3\text{-C m}^{-3}$ ) in the water, and  $b_{\text{CaCO}_3}(\lambda)$  is the effect on scattering of 1  $\text{mg CaCO}_3\text{-C m}^{-3}$ .

**3.2.2. Scattering by pure seawater and particulates.** The spectral variation in scattering by seawater is taken from Smith and Baker [1981]. The scattering due to noncalcite particulates (phytoplankton cells, detritus, noncalcite mineral particles) is calculated according to a formula similar to that suggested by Gordon and Morel [1983] but with an initial coefficient of 0.15 instead of 0.30

$$b_p(\lambda) = 0.15 \times (\text{chl})^{0.62} \times \left(\frac{550}{\lambda}\right) \quad (6)$$

The initial coefficient is halved because  $b_p(\lambda)$  normally includes coccolith scattering, but this is calculated separately here.

**3.2.3. Coccolith calcite scattering.** Previous work in the same northeast Atlantic bloom as studied here [Balch *et al.*, 1996b, Table 1] has deduced calcite-specific scattering impacts ( $b_{\text{CaCO}_3}$ ) of  $0.009371 \text{ m}^{-1} (\text{mg CaCO}_3\text{-C m}^{-3})^{-1}$  at 436 nm and  $0.008413 \text{ m}^{-1} (\text{mg CaCO}_3\text{-C m}^{-3})^{-1}$  at 546 nm. Comparable Gulf of Maine  $b_{\text{CaCO}_3}$  calculations [Balch *et al.*, 1991] for these two wavelengths (calculated assuming 30 coccoliths covering each cell and 0.25  $\text{pg CaCO}_3\text{-C coccolith}^{-1}$  [Tyrrell and Taylor, 1996, Table 3]) are  $0.009355 \text{ m}^{-1} (\text{mg CaCO}_3\text{-C m}^{-3})^{-1}$  at 436 nm and  $0.005847 \text{ m}^{-1} (\text{mg CaCO}_3\text{-C m}^{-3})^{-1}$  at 546 nm. These data are for coccoliths of *E. huxleyi*. The Gulf of Maine work also estimated  $b_{\text{CaCO}_3}$  for many other wavelengths in the 400–700 nm region [Balch *et al.*, 1991, Figure 8]. These pieces of information were combined to produce the model spectral calcite-specific scattering ( $b_{\text{CaCO}_3}(\lambda)$ ) shown in Figure 5 and Table 1.

During blooms of *Emiliania huxleyi*, many coccoliths become detached from the cells. The ratio of free coccoliths to cells can vary considerably across a bloom and with bloom age, with typical ratios of 20–200 [Holligan *et al.*, 1993; Garcia-Soto *et al.*, 1995]. The separate, suspended coccoliths have been thought in the past to contribute more strongly to the scattering than the coccoliths still attached to cells [Holligan *et al.*, 1983], but it has recently been calculated that particulate inorganic carbon (PIC), i.e., calcite summed over both attached and detached coccoliths, is a better predictor of the amount of scattering than is detached coccolith number [Balch *et al.*, 1996b]. In this study the scattering is calculated as a function of calcite concentration rather than of free coccolith number. Figure 4b shows the contributions of each component to scattering in the COPT model, for the case of 1.0 mg chl  $a$   $m^{-3}$  and 100.0  $\text{mg CaCO}_3\text{-C m}^{-3}$  in the water.

**3.2.4. Scattering phase function.** The standard (Petzold) scattering phase function [Mobley, 1994,

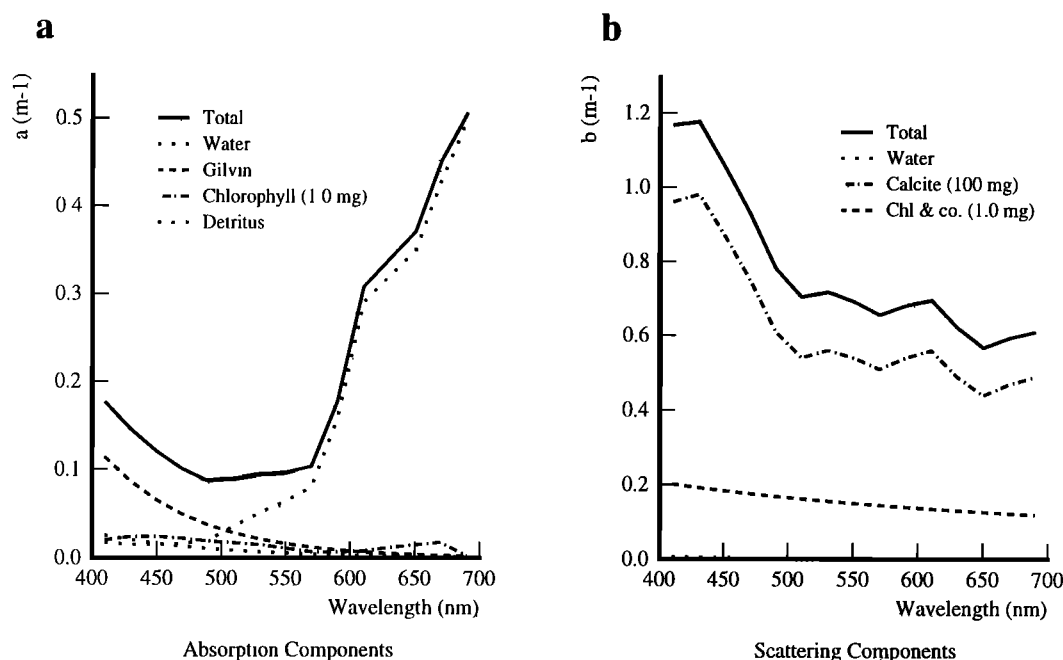


**Figure 4.** IOPs in the model. (a) Absorption spectra ( $\text{m}^{-1}$ ) for separate absorbing components and for total and (b) scattering spectra ( $\text{m}^{-1}$ ) for separate scattering components and for total. Coefficients are for  $1 \text{ mg chl } a \text{ m}^{-3}$  and  $100 \text{ mg CaCO}_3\text{-C m}^{-3}$ .

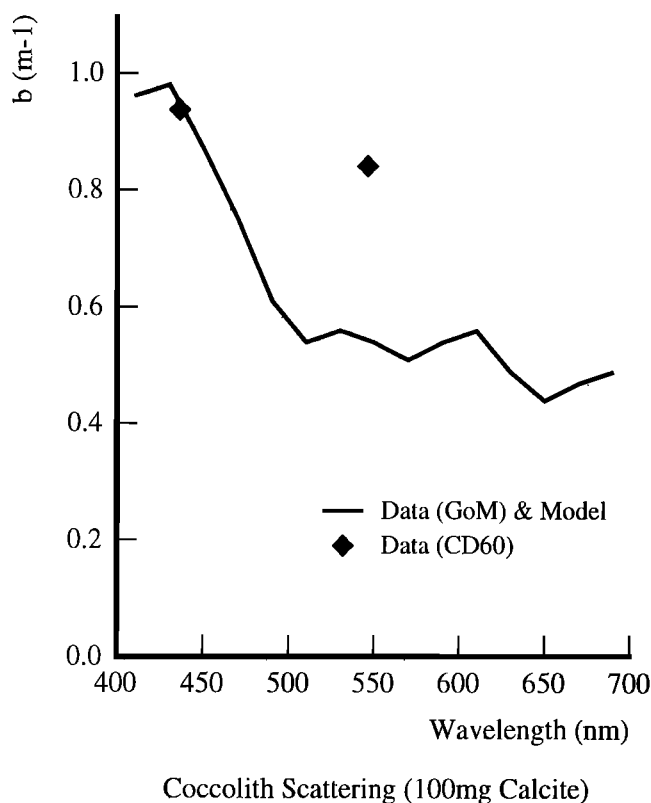


**Figure 5.** Coccolith-specific impact on scattering (per meter) at different wavelengths. Data are from the Gulf of Maine [Balch *et al.*, 1991, Figure 8] (calculated assuming 30 coccoliths covering each cell and  $0.25 \text{ pg CaCO}_3\text{-C coccolith}^{-1}$  [Tyrrell and Taylor, 1996, Table 3]), and the CD60 cruise to the northeast Atlantic [Balch *et al.*, 1996b, Table 1]. Calcite-specific scattering in the model is set equal to Gulf of Maine data.

Table 3.10, column 6] was used for all scattering components including calcite [Balch *et al.*, 1991], with the exception of water for which the scattering phase function was given the form [Mobley, 1994, p. 103]

$$\tilde{\beta}_w(\theta) = 0.06225 \times (1.0 + 0.835 \cos^2(\theta)) \quad (7)$$

The Petzold scattering phase function has a total scattering to backscattering ( $b:b_b$ ) ratio of 50, and this compares fairly well to (best fit slope of  $b$  against  $[\text{CaCO}_3]$  / best fit slope of  $b_b$  against  $[\text{CaCO}_3]$ ) from CD60 observations at 436 nm ( $b:b_b = 62$ ) and at 546 nm ( $b:b_b = 53$ ) [Balch *et al.*, 1996b, Table 1].

**3.2.5. Previous representations of calcite scattering.** The representation of coccolith scattering in the COPT model can be compared to that proposed by Gordon *et al.* [1988], which was formulated before Balch *et al.*'s [1996b] more detailed coccolith scattering data were available. Gordon *et al.* proposed that non-coccolith particulate scattering ( $b_p(\lambda)$ ) be calculated as for equation (6) above, but with an initial coefficient of 0.20 rather than 0.30, and also suggested that coccolith scattering ( $b_{\text{CaCO}_3}(\lambda)$ ) be calculated as a function of  $(1/\lambda^{2.5})$ .

Ackleson *et al.* [1994] followed a different approach in constructing the Gulf of Maine (GOM) model. Calcite scattering was split up into that due to attached coccoliths (lumped in with that due to chlorophyll) and that due to detached coccoliths (treated separately). Scattering due to both components was split up into forward and backward scattering contributions, to provide coefficients for a two-flow model. Backscattering and forward scattering by detached coccoliths were calculated using the equations

**Table 1.** Scattering Due to Coccoliths at a Concentration of 100 mg CaCO<sub>3</sub>-C m<sup>-3</sup> Versus Wavelength

$\lambda$ , nm	$b_{\text{CaCO}_3}(\lambda)$ , m <sup>-1</sup>
410	0.96
430	0.98
450	0.87
470	0.75
490	0.61
510	0.54
530	0.56
550	0.54
570	0.51
590	0.54
610	0.56
630	0.49
650	0.44
670	0.47
690	0.49

$$b_{b,\text{CaCO}_3}(\lambda) = 4.54 \times \text{CaCO}_{3,D} \times (\lambda^{-1.45}) \quad (8)$$

and

$$b_{f,\text{CaCO}_3}(\lambda) = 99.85 \times \text{CaCO}_{3,D} \times (\lambda^{-1.45}) \quad (9)$$

where CaCO<sub>3,D</sub> is the concentration of carbon in the form of detached coccoliths, in units of mg CaCO<sub>3</sub>-C m<sup>-3</sup>. The wavelength dependence of detached coccolith scattering in the GOM model was derived from fitting a curve to the same data [Balch *et al.*, 1991, Figure 8] as shown in Figure 5. A total scattering to backscattering ratio for detached coccoliths was derived for the GOM model by comparing estimates of total scattering and backscattering at 660 nm and then using this estimated ratio (= 23) over the whole spectra. This is in con-

trast to the Petzold ratio of 50 used here (section 3.2.4). Equation (8) above produces 0.0488 m<sup>-1</sup> backscattering at 546 nm with a concentration of 100 mg CaCO<sub>3</sub>-C m<sup>-3</sup>, approximately fourfold more than is obtained by taking the corresponding value from Table 1 and dividing it by 50.

#### 4. Model-Data Comparisons

Sections 2 and 3 have described the representation and testing of (1) optical processes and (2) IOPs in the COPT model. The IOPs were set up to be variable as functions of chlorophyll and calcite. COPT model predictions were then compared with data from six stations during the CD60 cruise, those stations where optical casts were carried out at the same time as chlorophyll and calcite measurements were made. The comparisons involved three steps: (1) The values of chlorophyll and calcite in the model were taken from bottle measurements and from calibrated chlorophyll fluorescence measurements and were then checked against beam transmissometer measurements made at the stations; (2) appropriate values for relevant meteorological parameters were obtained for each station (from shipboard measurements) and used to parameterize the model run for that station; and (3) the resulting model outputs were compared with the in situ measured scalar irradiances ( $E_{\text{od}}$  and  $E_{\text{ou}}$ ) and with calculated apparent optical properties (AOPs) ( $K_{\text{od}}$  and  $R_{\text{o}}$ ).

Table 2 shows the parameters used to force the COPT model runs at each station. Model chlorophyll and calcite concentrations are estimated from data as shown in Figure 6.

The results obtained are shown in Figure 7, together with the comparisons with field observations. The model-data comparisons are evaluated in section 6.1.

**Table 2.** CD60 Station Descriptions

Location (°N,°W)	Date in June 1991	Time (local)	Sun Angle $\theta$	$E_{\text{d}}(\text{air})$		Cloud, %	Wind, m s <sup>-1</sup>	Chl <i>a</i> , mg m <sup>-3</sup>	PIC, mg CaCO <sub>3</sub> -C m <sup>-3</sup>
				Clear Sky, W m <sup>-2</sup>	Measured, W m <sup>-2</sup>				
(58, 20)	18	0816	52°39'	504	400	70	5	1.0	43
(62, 20)	20	1348	42°38'	680	670	0	1	1.0	280
(62, 23)	22	0743	57°26'	410	130	95	6	0.75	240
(60, 21)	26	0747	56°35'	427	130	100	8	1.2	64
(61, 15)	27	1527	51°48'	520	200	90	9	2.3	115
(61, 16)	29	1319	40°12'	720	500	75	2	1.1	140

PIC, particulate inorganic carbon. Zenith angle is calculated from simple astronomical equations [Kirk, 1994]. Theoretical clear-sky, sea-surface, total downward irradiance values (summed over all wavelengths, not just PAR) are estimated by multiplying the solar constant by the cosine of the solar zenith angle, and then by removing a proportion to account for transmission loss through the atmosphere (24% for an overhead Sun, proportionately more for longer pathlengths when the Sun is lower in the sky) [Kirk, 1994]. Cloud cover is estimated from the difference between the theoretical clear-sky and the observed above-surface downward irradiances in the columns labeled  $E_{\text{d}}(\text{air})$ . Actual downward irradiances and wind velocities are taken from the underway data set in the Biogeochemical Ocean Flux Study (BOFS) CD-ROM. The estimation of chlorophyll *a* and calcite concentrations from data is shown in Figure 6.

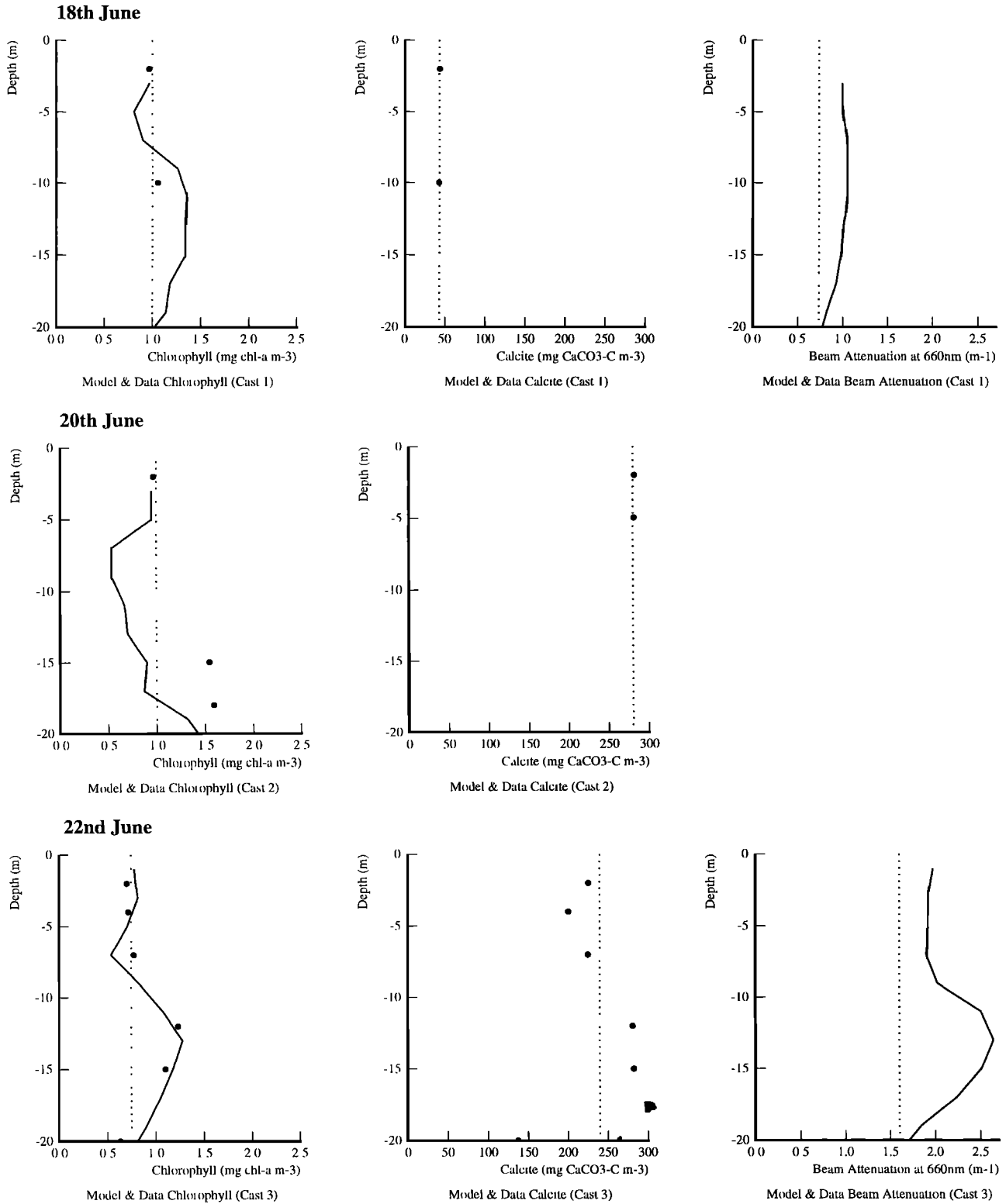


**Figure 6.** Model and data IOP comparisons for the six CD60 stations described in Table 2. Each row corresponds to a different station, in the same order as in Table 2. Model values (constant through the top 20 m) are shown as dashed lines, data profiles are shown as solid lines, and single data measurement values are shown as solid circles. (left) Comparison of chlorophyll concentrations ( $\text{mg chl } a \text{ m}^{-3}$ ) with the solid line obtained from in vivo chlorophyll fluorescence and the solid circles obtained from chlorophyll fluorescence of extracted pigments. (middle) Comparison of coccolith calcite concentrations ( $\text{mg CaCO}_3\text{-C m}^{-3}$ ). (right) Comparison of  $c_{660}$  values ( $\text{m}^{-1}$ ) with the solid line obtained from beam transmissometer measurements (no measurements at second station).

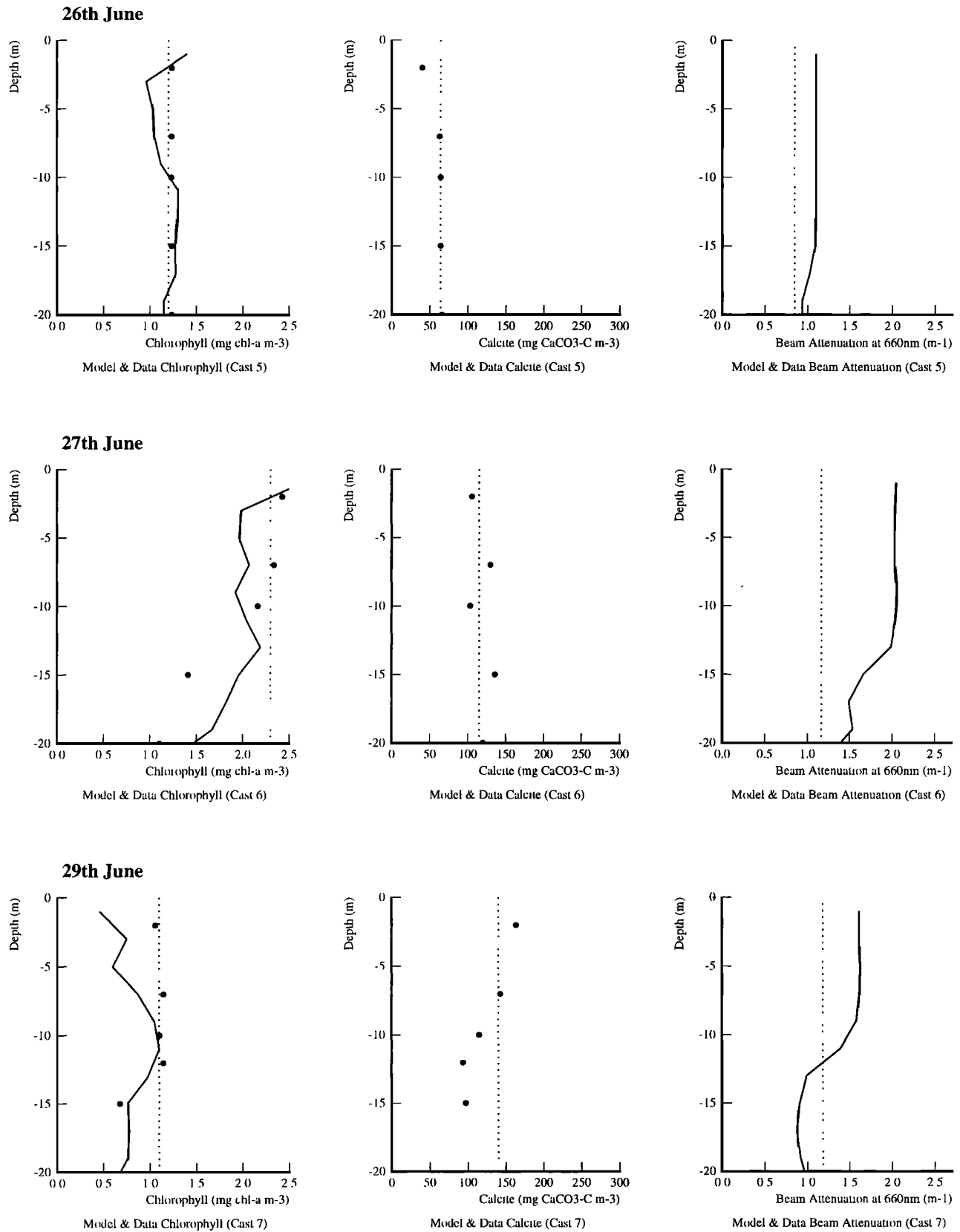
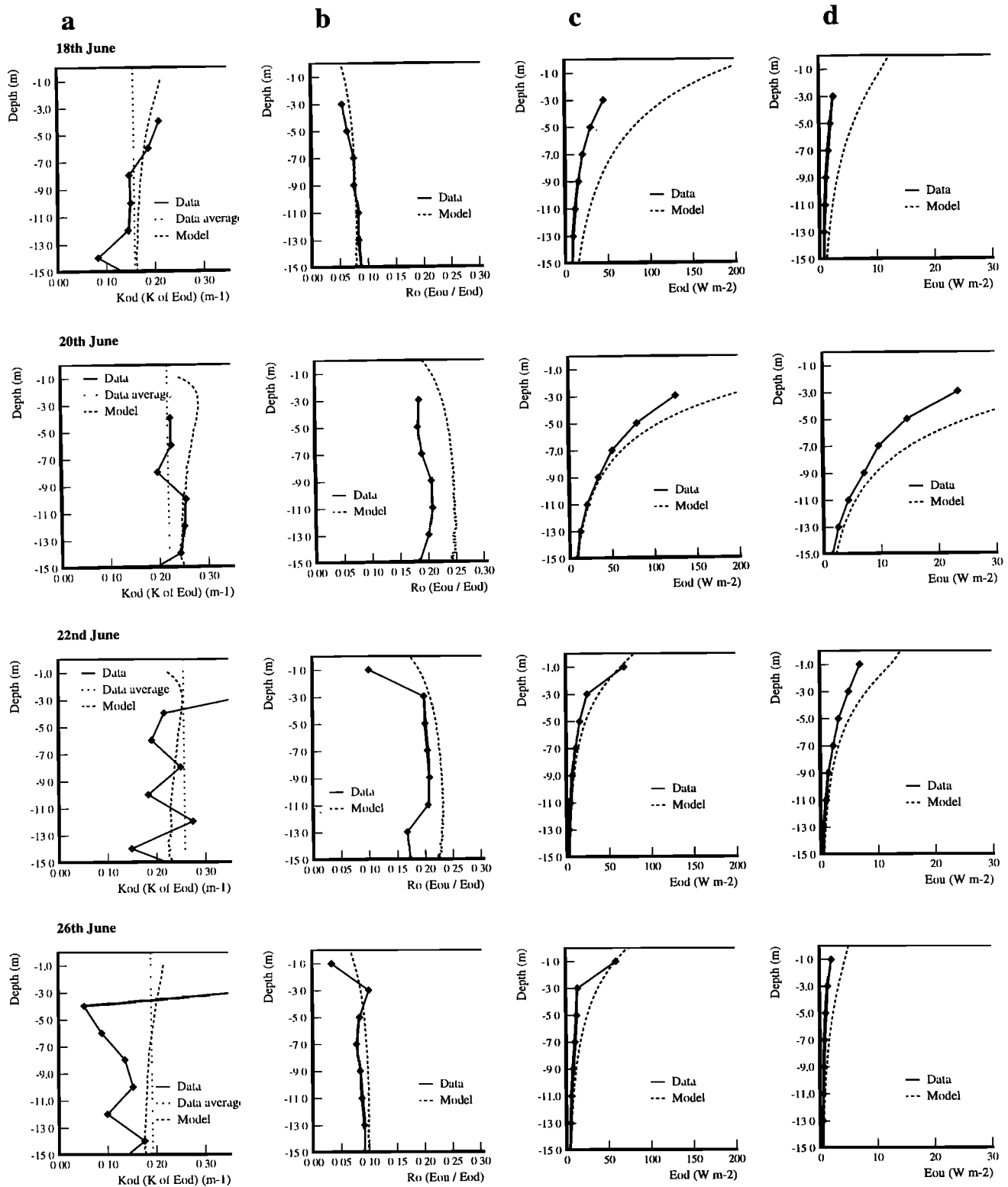


Figure 6. (continued)



**Figure 7.** Model (COPT) and data AOP comparisons for the six CD60 stations described in Table 2. Each row corresponds to a different station, in the same order as in Table 2. Model profiles are again shown as dashed lines and measurements are shown as solid diamonds connected by solid lines. (a) Comparison of  $K_{0d}$  values (vertical attenuation coefficients for downwelling scalar irradiances) ( $m^{-1}$ ), with data  $K_{0d}$  values calculated from adjacent  $E_{0d}$  values and with the average data  $K_{0d}$  in the top 15 m shown as a vertical dotted line. (b) Comparison of in-water scalar irradiance reflectances ( $R_0 = E_{0u} / E_{0d}$ ). (c)-(d) Comparisons of  $E_{0d}$  values (downward scalar irradiances) and  $E_{0u}$  values (upward scalar irradiances) (both  $W m^{-2}$ ). All irradiances (and therefore derived values) are for summations over 400-700 nm (PAR).

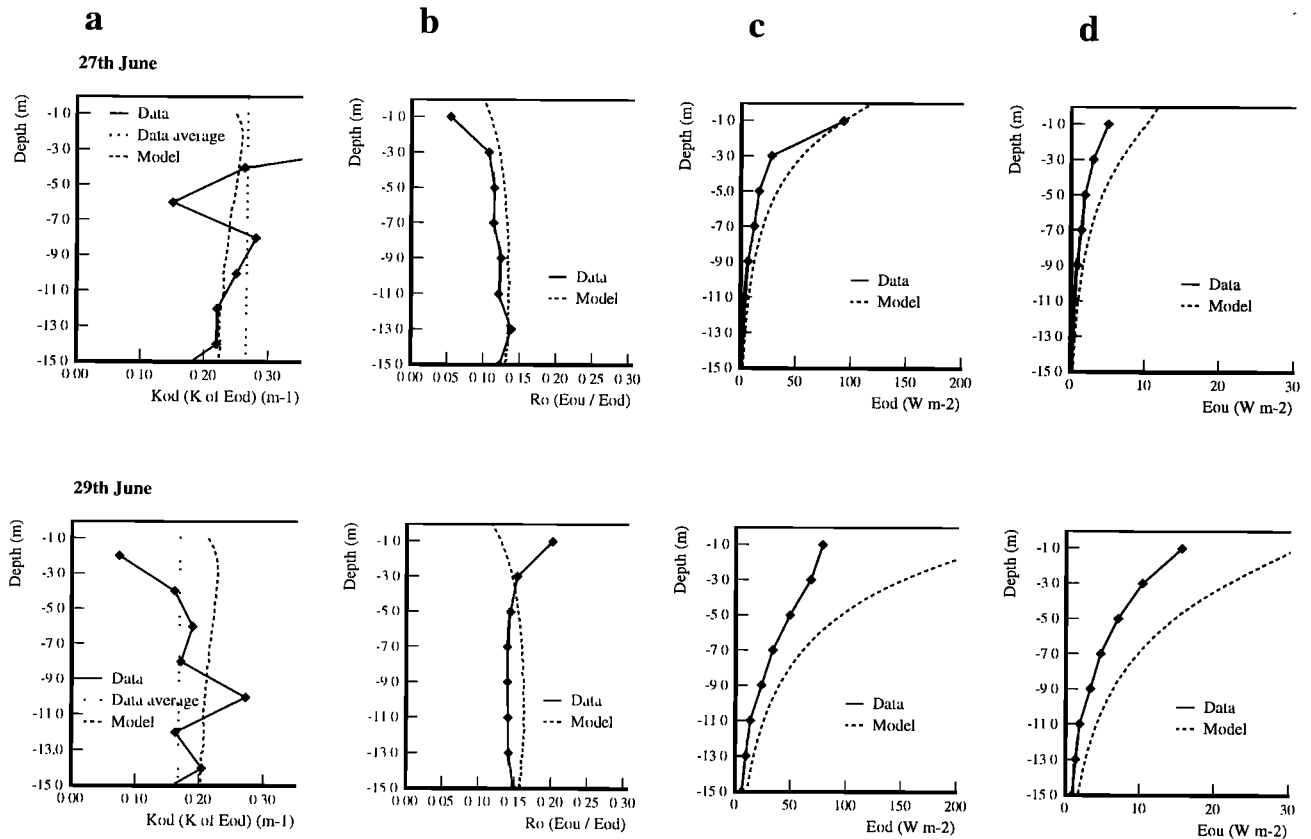


Figure 7. (continued)

## 5. Model Estimates of Many Optical Properties

The model-data comparisons of Figure 7, together with the model-model comparisons described earlier, served to validate the COPT Monte Carlo model used here. With the confidence gained from these validation steps, COPT was then used to predict many aspects of the bloom optics that were not measured at the time.

For all of the model results below, the Sun is at 45° (corresponding to 0930 or 1430 local time on June 15 at 60°N), the wind speed is 5 m s<sup>-1</sup>, and there is 25% cloud. Sensitivity analyses (section 6.4) verified that the model AOPs are not greatly affected by wind speed, by cloud cover, or by solar zenith angle if  $\theta < 60^\circ$ . Cloud cover and sun zenith angle obviously have a major impact on the magnitude of the downward irradiance arriving at the water surface ( $E_d(\text{air})$ ), and therefore on the magnitude of the in-water irradiances and radiances, but they do not greatly affect AOPs such as  $K_d$  or  $R$ . All irradiances and AOPs shown in Figure 7 and elsewhere in the paper are summed or averaged over all photosynthetically active radiation (PAR, 400–700nm), rather than being for specific wavelengths. PAR AOPs or irradiances are calculated in the model by first calculating the values at representative wavelengths (410, 430, 450, ... 690 nm) and then finally by averaging or summing the values at each wavelength, with the value at each wavelength being weighted by the amount of incident irradiance in that part of the spectrum.

### 5.1. In the Water

The first set of COPT model outputs (Figure 8) show total scalar, downward, and upward irradiances, reflectances, vertical attenuation rates, and average cosines for four different calcite concentrations (0, 100, 200, and 300 mg CaCO<sub>3</sub>-C m<sup>-3</sup>) at a constant chlorophyll *a* concentration of 0.75 mg chl *a* m<sup>-3</sup>. The second set of COPT model outputs (Figure 9) show the same optical variables, this time for a variable chlorophyll *a* concentration (0.1, 1.0, 2.0, and 3.0 mg chl *a* m<sup>-3</sup>) at a constant calcite concentration of 100 mg CaCO<sub>3</sub>-C m<sup>-3</sup>. The enhancement of near-surface irradiance in the presence of intense scattering is in accordance with theoretical predictions [Stavn *et al.*, 1984; Plass *et al.*, 1981] and is equally apparent in both COPT and HYDROLIGHT results. Table 3 shows the shading effect of the coccolith scattering on the light availability at 15 m depth, a depth at which a thermocline phytoplankton population (deep chlorophyll maximum) might otherwise start to form at that time of year.

### 5.2. Above the Water

Table 4 shows the impact of chlorophyll and calcite on the emergent flux, where the emergent flux consists of those photons entering the water which later leave it again following scattering. Figure 10 also portrays the directional emergent flux (radiance) in the absence and presence of coccoliths. Figure 11 shows the change in the vertical upward water-leaving radiance (the nadir radiance,  $L_u\text{-out}$ ) as a function of calcite at constant

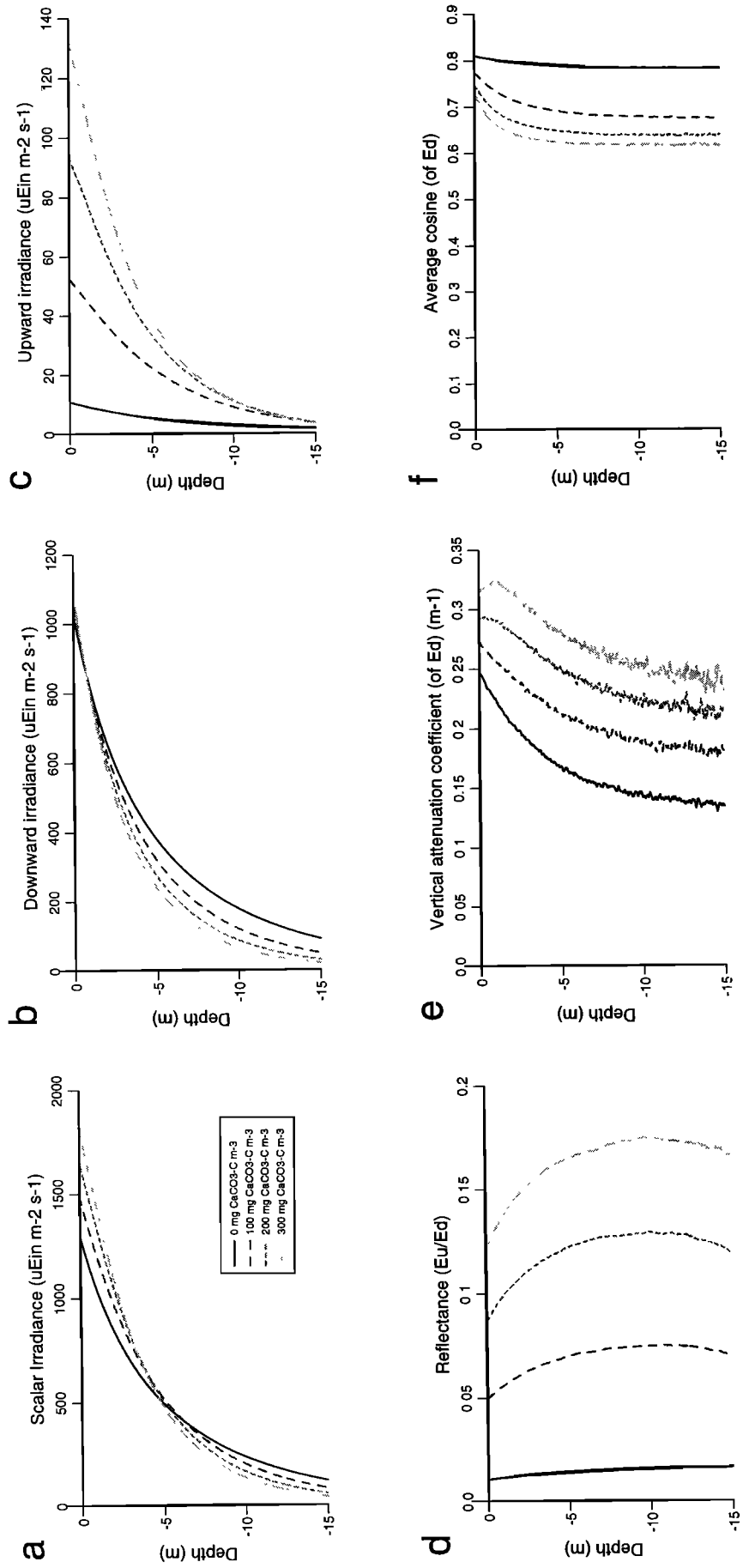


**Figure 8.** COPT model predictions of optical effects of coccolith calcite is varied between 0 and 300 mg CaCO<sub>3</sub>-C m<sup>-3</sup>, while all other parameters are kept constant at chlorophyll = 0.75 mg chl a m<sup>-3</sup>,  $\theta = 45^\circ$ ,  $E_d(\text{air}) = 1100 \mu\text{Ein m}^{-2} \text{s}^{-1}$ , wind speed = 5 m s<sup>-1</sup>, and cloud cover = 25%. (a)  $E_o$ , (b)  $E_d$ , (c)  $E_u$ , (d)  $R$ , (e)  $K_d$ , and (f)  $\bar{\mu}_d$  are shown. Monte Carlo fluctuations are apparent in the results, particularly in Figure 8e.

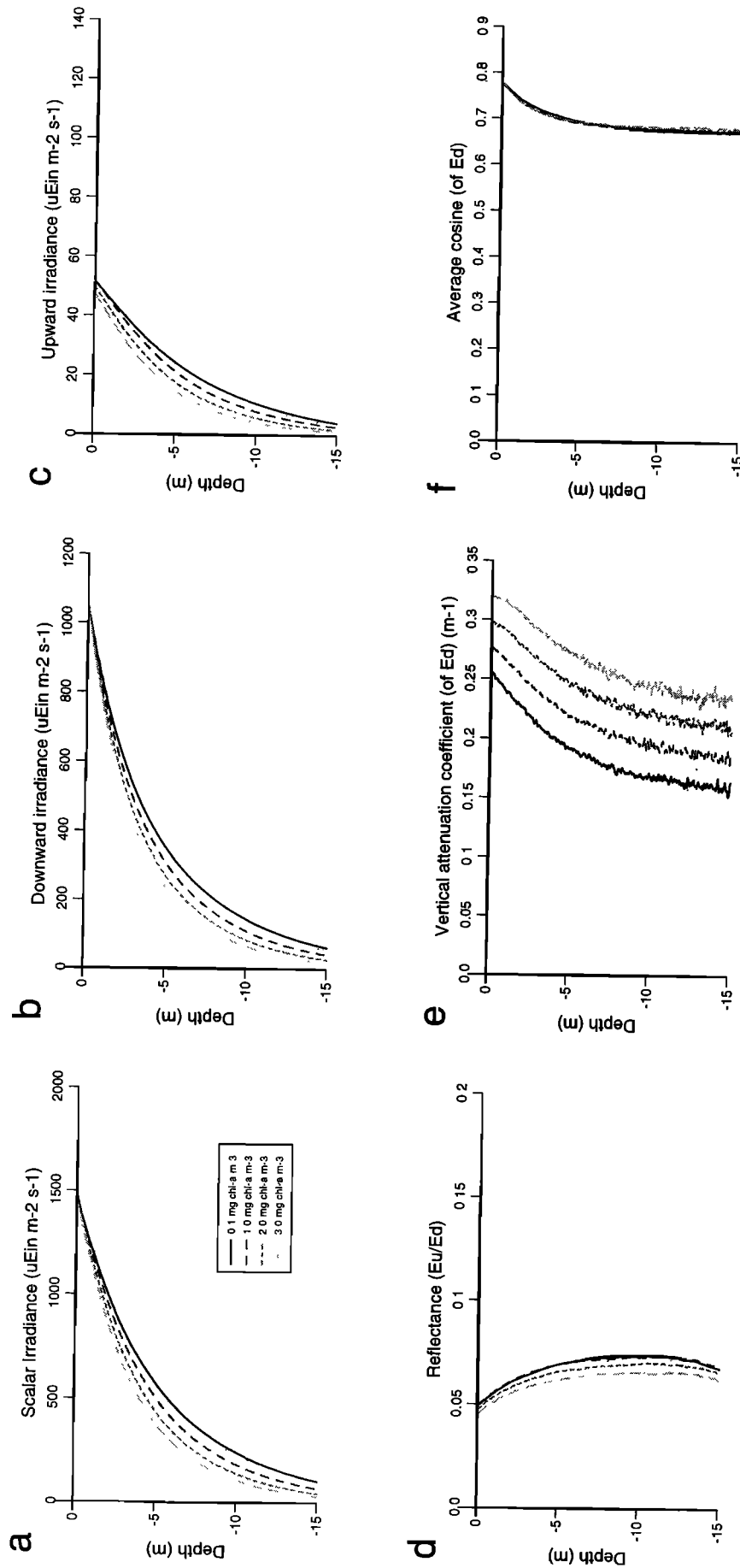


**Figure 9.** COPT model predictions of optical effects of chlorophyll. The concentration of chlorophyll is varied between 0.1 and 3.0 mg chl  $a$   $m^{-3}$ , while all other parameters are kept constant at calcite = 100.0 mg  $CaCO_3-C$   $m^{-3}$ ,  $\theta = 45^\circ$ ,  $E_d(\text{air}) = 1100 \mu\text{Ein } m^{-2} s^{-1}$ , wind speed = 5  $m s^{-1}$  and cloud cover = 25%. (a)  $E_0$ , (b)  $E_d$ , (c)  $E_u$ , (d)  $R$ , (e)  $K_d$ , and (f)  $\bar{\mu}_d$  are shown. Monte Carlo fluctuations are apparent in the results, particularly in Figure 9e.

**Table 3.** Scalar Irradiance at 15 m Depth for Varying Concentrations of Calcite and Chlorophyll (COPT Model Predictions)

Chlorophyll	Calcite			
	0.0	100.0	200.0	300.0
0.0	158	114	79	57
0.5	129	88	61	43
1.0	107	71	48	34
1.5	88	58	39	27
2.0	74	48	32	22

Values are in units of  $\mu\text{Ein m}^{-2} \text{s}^{-1}$ .

chlorophyll and as a function of chlorophyll at constant calcite.  $L_u$ -out is not always a monotonic function of chlorophyll because chlorophyll both absorbs and scatters photons.

### 5.3. Photon Budgets

Figure 12 shows the various fates of the photon population under three different calcite concentrations (0, 100, and 300  $\text{mg CaCO}_3\text{-C m}^{-3}$ ) at a constant chlorophyll  $a$  concentration (0.75  $\text{mg chl } a \text{ m}^{-3}$ ). These photon budgets show the proportions of photons (as a percentage of the incident flux which hits the top of the water surface), which end up (1) being absorbed by the water or (2) by chlorophyll; the proportions being returned to the atmosphere by (3) surface reflection or (4) internal scattering; and (5) the proportions penetrating through to below the mixed layer (to  $>20$  m depth).

## 6. Discussion

### 6.1. "Tuning" of the Model

In assessing the fit between model and data, the following points should be borne in mind:

1. The model assumes constant chlorophyll and calcite (as well as other components) in a homogeneous layer down to 20 m depth, whereas in reality it can be seen (Figure 6) that there is some vertical vari-

**Table 4.** Emergent Flux (Percentage of Photons Reemitted Upward Out of the Water) Relative to the Incident Photon Flux, for Varying Concentrations of Calcite and Chlorophyll (COPT Model Predictions)

Chlorophyll	Calcite			
	0.0	100.0	200.0	300.0
0.0	0.17	1.84	3.74	5.52
0.5	0.37	1.96	3.69	5.38
1.0	0.44	1.94	3.54	5.09
1.5	0.49	1.89	3.40	4.85
2.0	0.54	1.84	3.25	4.62

ability in these components, even within the top 20 m.

2. The model assumes a constant surface illumination for each profile when generating estimates of subsurface irradiances. However, examination of the minute-by-minute surface radiation data shows that the intensity of the sunlight varied significantly during some of the conductivity-temperature-depth (CTD) optical casts, which took up to 30 min to perform. Time stamping of individual CTD optical measurements was not available in the data set but would have assisted interpretation if present.

3. The optical sensors were calibrated to the same standard lamp before the CD60 cruise and correctly zeroed, and so measurements should therefore be reliable for determination of  $K_{od}$  and  $R_o$  values. However, uncertainties in the output of the reference lamp meant that absolute values of irradiances may not be reliable (G. Moore, personal communication, 1997).

4. Several components (e.g., gilvin and detritus) were assumed not to vary from one station to another, whereas there may have been some variation.

Figures 6 and 7 show that the overall agreement between model results and observations is reasonable except for  $E_{od}$  and  $E_{ou}$ . For some stations the magnitude of the observed in-water scalar irradiances ( $E_{od}(z)$  and  $E_{ou}(z)$ ) seemed incompatible with observed above-surface irradiances (both  $E_{od}(\text{air})(\text{PAR})$  and  $E_d(\text{air})(\text{total})$ ), perhaps as a result of the incomplete sensor calibration mentioned above. Hence it was not found possible to obtain a good fit between data and model  $E_{od}$  and  $E_{ou}$  values, when the model irradiances were driven by observed above-surface irradiance measurements.

It was also not found to be possible to accurately fit  $K_{od}$ ,  $R_o$ , and  $c_{660}$  values simultaneously for all stations. Optimization was carried out by varying the least constrained constituents, the noncoccolith particulate scattering and the absorption due to gilvin (within a range of likely values), to improve the model-data fit. Although  $b_p(\lambda)$  and  $a_g(\lambda)$  were partially "tuned", the same parameterization was used at each of the six stations. The only aspects of the model IOPs that varied between stations were the chlorophyll and calcite concentrations and these were forced from data.

$K_{od}$  data and model values agree well. Values of  $c_{660}$  and  $R_o$  increase at high coccolith concentrations in both observations and model results. However, the  $R_o$  comparisons (particularly June 20 and 22) suggest that the model overestimates coccolith scattering, whereas the  $c_{660}$  comparisons suggest, if anything, the opposite. Because the model-data comparison shows a reasonable fit and does not give clear evidence of a poor representation of coccolith scattering, the model coccolith scattering shown in Figure 5 (based on the data of Balch) is left unchanged.

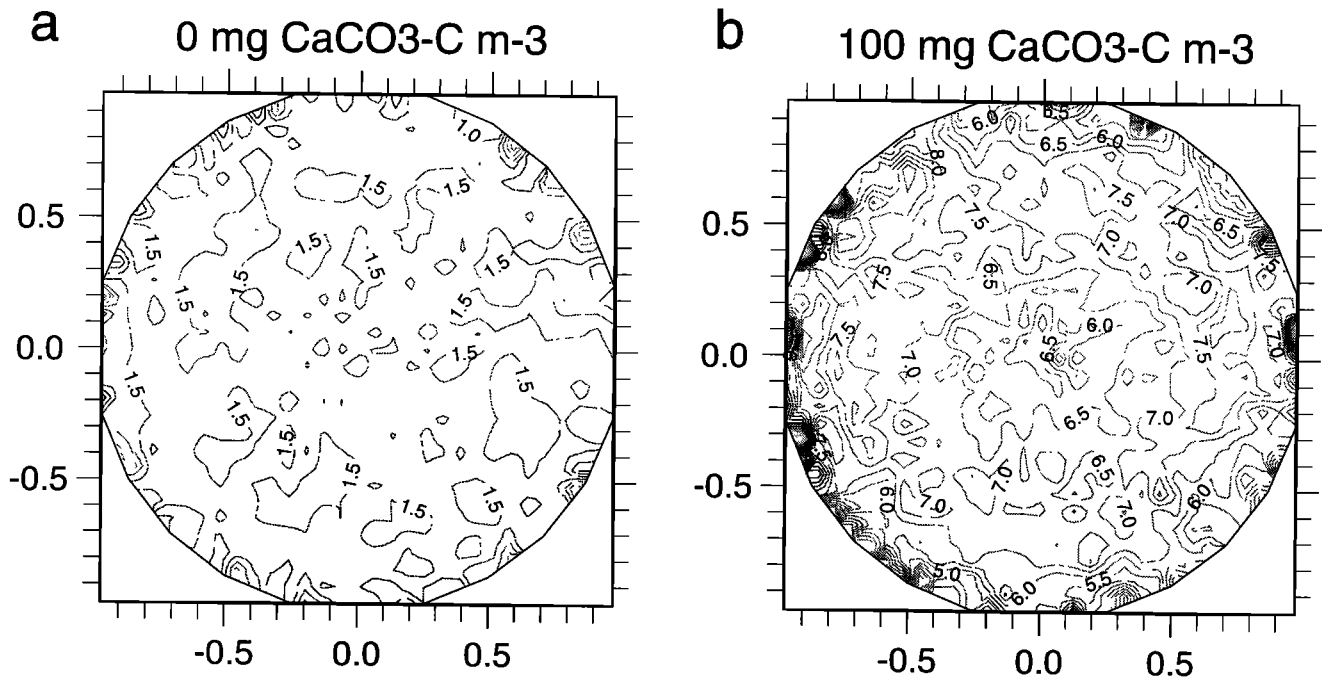


**Figure 10.** Emergent flux, i.e., water-leaving radiance ( $\mu\text{Ein m}^{-2} \text{s}^{-1} \text{sr}^{-1}$ ), as calculated by the COPT model for two calcite concentrations of (a) 0 and (b) 100  $\text{mg CaCO}_3\text{-C m}^{-3}$ , with other parameters constant at chlorophyll =  $0.75 \text{ mg chl } a \text{ m}^{-3}$ ,  $\theta = 45^\circ$ ,  $E_d(\text{air}) = 1100 \mu\text{Ein m}^{-2} \text{s}^{-1}$ , wind speed =  $5 \text{ m s}^{-1}$  and cloud cover = 25%. Variability is due to Monte Carlo fluctuations.

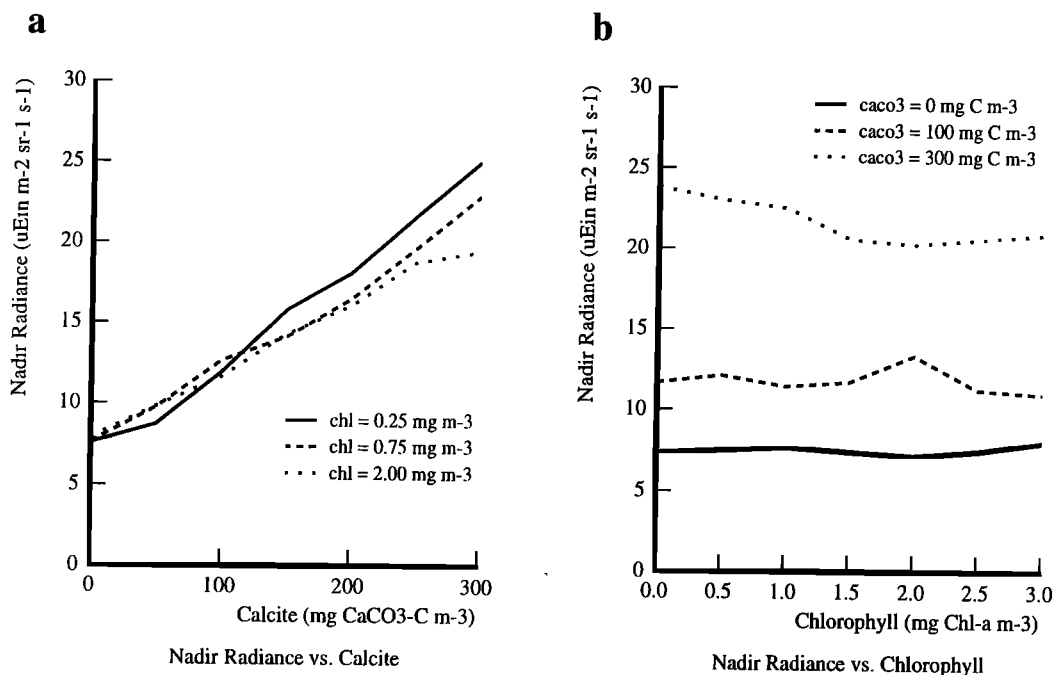


**Figure 11.** COPT model calculated nadir (vertical upward) water-leaving radiance ( $L_{u\text{-out}}$ , units of  $\mu\text{Ein m}^{-2} \text{s}^{-1} \text{sr}^{-1}$ ) as a function of (a) calcite concentration ( $\text{mg CaCO}_3\text{-C m}^{-3}$ ) with chlorophyll constant at  $0.75 \text{ mg chl } a \text{ m}^{-3}$  and (b) chlorophyll concentration ( $\text{mg chl } a \text{ m}^{-3}$ ) with calcite constant at  $100.0 \text{ mg CaCO}_3\text{-C m}^{-3}$ . Other parameters kept constant at  $\theta = 45^\circ$ ,  $E_d(\text{air}) = 1100 \mu\text{Ein m}^{-2} \text{s}^{-1}$ , wind speed =  $5 \text{ m s}^{-1}$ , and cloud cover = 25%.

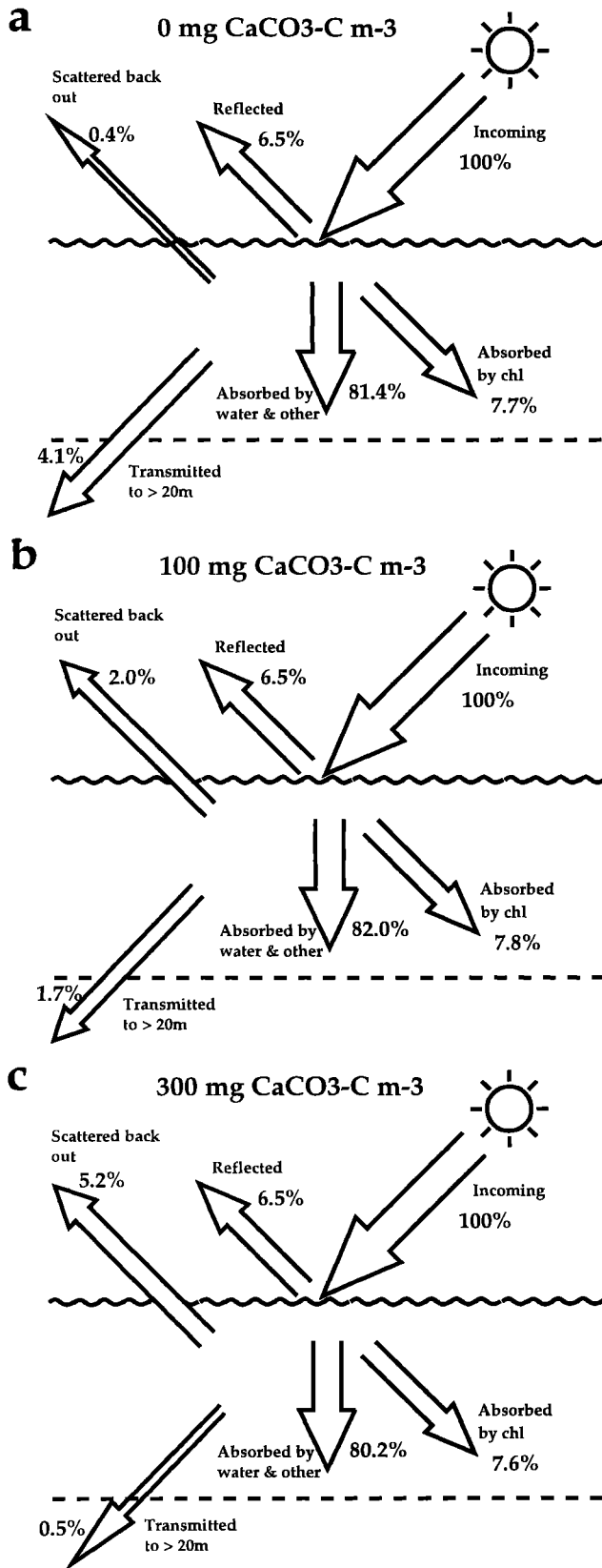


**Figure 12.** Photon budgets (calculated using COPT) for (a) 0 mg  $\text{CaCO}_3\text{-C m}^{-3}$ , (b) 100 mg  $\text{CaCO}_3\text{-C m}^{-3}$ , and (c) 300 mg  $\text{CaCO}_3\text{-C m}^{-3}$ . Other parameters are chlorophyll = 0.75 mg chl  $a \text{ m}^{-3}$ ,  $\theta = 45^\circ$ ,  $E_d(\text{air}) = 1100 \mu\text{Ein m}^{-2} \text{ s}^{-1}$ , wind speed = 5 m  $\text{s}^{-1}$  and cloud cover = 25%.

## 6.2. Main Coccolith Perturbations to Optics

From the results shown in section 6.1, the coccolith-induced changes to light in the ocean can be summarized as follows:

1. The surface water (the top few meters) becomes brighter.
2. The rate of extinction of light with depth is increased.
3. Deeper water (below the top few meters) becomes darker.
4. Seen from above, the ocean is brighter (it has a higher albedo).

## 6.3. Effects Depend on Chlorophyll as Well as Calcite

From Figures 8 and 9, it is apparent that the optical impacts due to coccoliths are not solely dependent on the number of coccoliths in the water (the concentration of calcite). Rather, the optical impacts also vary according to how much chlorophyll is in the water. This is to be expected, given that  $K_d$  is a positive function of both  $a$  and  $b$  [Kirk, 1994, p. 160–168] and  $R$  is also a function of  $(b/a)$  [Kirk, 1994, Figure 6.16]. In general, the optical behavior of the ocean is a function of both  $a$  and  $b$ . It should be noted that the modeling assumes that chlorophyll has constant absorbing and scattering properties. Species-dependent variations in the relative proportions of different pigments, and therefore in  $(b/a)$ , are not considered.

## 6.4. Other Factors: Sensitivity Analyses

Other factors also influence the light in the ocean, including the angular and spectral composition (not just the magnitude) of the incident light that hits the sea surface. The following sensitivity analyses were carried out

1. The atmospheric downward irradiance just above the sea surface  $E_d(\text{air})$  was held constant (1100  $\mu\text{Ein m}^{-2} \text{ s}^{-1}$ ), as was chlorophyll (0.75 mg chl  $a \text{ m}^{-3}$ ), calcite (100 mg  $\text{CaCO}_3\text{-C m}^{-3}$ ), wind speed (5 m  $\text{s}^{-1}$ ), and cloudiness (25%). At the same time,  $\theta$  was varied between  $0^\circ$  and  $80^\circ$ . It was observed from the model results that zenith angle does not have a great effect on the in-water AOPs (not shown), provided the zenith angle is not greater than about  $60^\circ$  from the vertical (maximum change to  $R$  or  $K_d = 10\%$ ).
2. Conditions were as for (1), except that  $\theta$  was held constant at  $45^\circ$ , while the cloudiness was varied between 0 and 100%. The model results showed that the degree of cloudiness (and the change in the ratio of diffuse to direct sunlight that is brought about) does not greatly affect the AOPs (maximum change to  $R$  or  $K_d = 5\%$ ).
3. Conditions were as for (1), except that  $\theta$  was held constant at  $45^\circ$ , while wind speed was varied between 0 and 20 m  $\text{s}^{-1}$ . The degree of wind-

roughening of the sea surface was shown to be of relatively minor importance (maximum change to  $R$  or  $K_d = 6\%$ ).

Other processes also play minor roles in determining the nature of the underwater light field but have been ignored here. These include chlorophyll fluorescence, colored dissolved organic matter (CDOM) fluorescence, and Raman scattering. Including these processes in a model run of HYDROLIGHT (given the same meteorological conditions and in-water IOPs as COPT) made negligible differences to the results.

Two other sensitivity analyses examined the effect on model predictions of assuming constant IOPs with depth, when the IOPs are in fact variable with depth. Model calculations of irradiances and AOPs were made with HYDROLIGHT for the CD60 casts on June 22 and 29 (for which IOPs changed significantly with depth), using both (1) vertically constant IOPs (as in Table 2) and (2) depth-variable IOPs obtained by interpolation and extrapolation from the point measurements of chlorophyll and calcite shown in Figure 6. The maximum differences between (1) and (2) for either station were  $E_d(z)$ , 5%;  $E_u(z)$ , 14%;  $K_d(z)$ , 5%;  $R(z)$ , 13%; and  $E_u(\text{air})$ , 5%.

### 6.5. Nepheloid Layers

Most of the effects of a coccolith bloom in the surface mixed layer are also apparent in a subsurface nepheloid layer, i.e., a distinct layer containing scattering particles such as coccoliths. Figure 13 shows the HYDROLIGHT model-predicted perturbations to scalar irradiance caused by adding a scattering layer (corresponding to  $500 \text{ mg CaCO}_3\text{-C m}^{-3}$ ) between 5 m and 7 m. It can be seen that the thin scattering layer increases scalar irradiance within the layer and also above the layer but shades the water beneath it. It should be noted that, with respect to the increase in scalar irradiance with depth at the top of the coccolith layer, scalar photon flux is not a conservative quantity.

### 6.6. Impact on Habitability of the Surface Ocean

Phytoplankton require sunlight in order to photosynthesize. At low light intensities respiration tends to exceed photosynthesis so that survival is not possible. The minimum light requirement for phytoplankton survival in the ocean (the "compensation point") is typically considered to be about 1% of the surface light intensity, i.e., of the order of  $10 \mu\text{Ein m}^{-2} \text{ s}^{-1}$  for a surface light intensity of  $1000 \mu\text{Ein m}^{-2} \text{ s}^{-1}$ . For diatoms the compensation point has been quoted as  $1.5\text{--}1.7 \text{ W m}^{-2} \approx 7 \mu\text{Ein m}^{-2} \text{ s}^{-1}$  [Mann and Lazier, 1991, p. 86]. In the model the depth at which scalar light intensity falls to 1% of the surface value decreases from  $\sim 52 \text{ m}$  in the absence of coccoliths to  $\sim 26 \text{ m}$  when they are present at a concentration of  $100 \text{ mg CaCO}_3\text{-C m}^{-3}$ , although these depths are probably overestimated because there is no

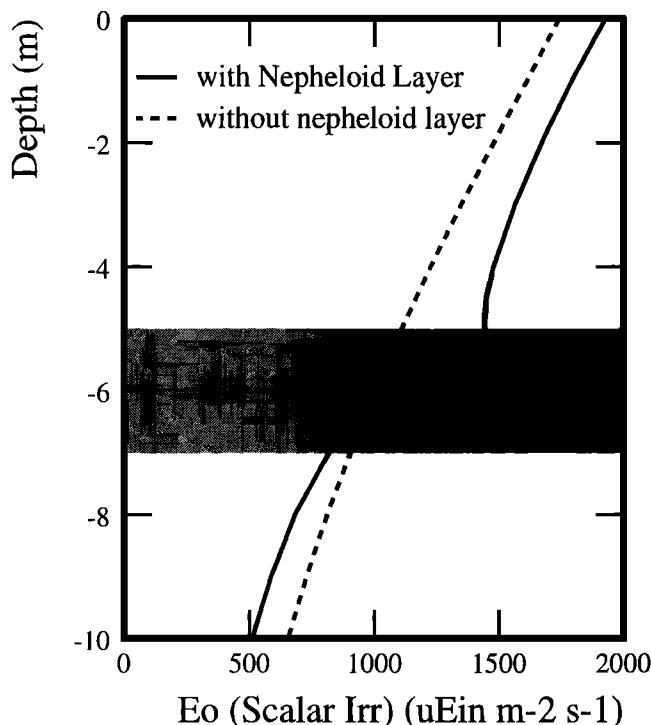


**Figure 13.** Effects of a nepheloid layer on  $E_o$ : HYDROLIGHT model simulation of the impact of a distinct scattering layer of coccoliths, at a concentration of  $500 \text{ mg CaCO}_3\text{-C m}^{-3}$ , between 5 and 7 m depth. The solid line shows the depth profile of  $E_o$  when the subsurface layer of coccoliths is present (no coccoliths except between 5 and 7 m), in contrast to the dashed line showing the  $E_o$  profile when there are no coccoliths at all present in the water. Other parameters are chlorophyll =  $0.75 \text{ mg chl a m}^{-3}$ ,  $\theta = 45^\circ$ ,  $E_d(\text{air}) = 1300 \mu\text{Ein m}^{-2} \text{ s}^{-1}$ , wind speed =  $5 \text{ m s}^{-1}$ , and cloud cover = 25%. The IOPs at each depth are identical for the two model runs, except for  $b(\lambda)$  between 5 and 7 m.

attenuation below 20 m in the model except that due to water. In other words, a strong bloom of *Emiliania huxleyi* causes (intense) shading of the water beneath it, thus raising the "compensation depth." The 1% isolume has previously been estimated to change from " $>24 \text{ m}$  outside the bloom to as low as 8 m in the most turbid water" [Holligan *et al.*, 1993] and from " $\sim 45 \text{ m}$  (during nonbloom periods) to 20 m during a bloom" [Balch *et al.*, 1991], where in both cases the maximum calcite concentration was greater than the  $100 \text{ mg CaCO}_3\text{-C m}^{-3}$  used above.

A strong concentration of coccoliths will cause increased heating of surface waters (above 5 m) and decreased heating of deeper waters, thereby increasing the strength of the stratification and reducing vertical mixing. Coccolith light scattering will thereby inhibit the upward flow of nutrients due to mixing with deeper water. Taken together, these effects are likely to mean that coccolith-laden water is less favorable for phytoplankton growth than otherwise, and this may partly explain the

low levels of chlorophyll often associated with coccolith-rich waters [e.g., *Garcia-Soto et al.*, 1995; *Holligan et al.*, 1993].

Coccoliths also increase the near-surface brightness (Figure 8a), and this can induce photoinhibition. If it is assumed that photoinhibition becomes important above  $\sim 1000 \mu\text{Ein m}^{-2} \text{s}^{-1}$  (see *Kirk* [1994]; although see *Nanninga and Tyrrell* [1996] for possible lack of photoinhibition in *E. huxleyi*), then in the middle of a partially overcast (25% cloud) day in June at  $60^\circ\text{N}$ , the top 1.9 m of the water will be photoinhibited when coccoliths are present at  $100 \text{ mg CaCO}_3\text{-C m}^{-3}$ , whereas only the top 1.2 m will be photoinhibited if they are absent (Figure 8a). This effect will combine with the shallowing of the compensation depth to reduce the total productivity of the system.

### 6.7. Climatological Impact

Heating rates are proportional to scalar irradiances (the photon flux, counting photons traveling in all directions equally). As discussed above, high coccolith concentrations promote stratification. It is likely that they also cause a reduction in the amount of absorbed heat that is ultimately retained by the ocean. Heat that is absorbed near to the surface (these model results, as well as observations [*Ackleson et al.*, 1988], suggest that high coccoliths cause warmer surface water) will be more easily lost back to the atmosphere, especially at night. In addition, as the photon budgets in Figure 12 show, more photons are returned to the atmosphere following subsurface scattering, and this also reduces the overall heating of the water.

What is the effect of coccolith scattering on the albedo of the entire water body ( $A = E_n(\text{air})/E_c(\text{air})$ )? This water body albedo should be distinguished [*Mobley*, 1994, p. 193–194] from the irradiance reflectance of the water surface for downward traveling photons ( $r_+$ ) and in-water reflectance ( $R(z) = E_n(z)/E_d(z)$ ).  $A$  is made up of both  $r_+$  and the photons traveling back up and out of the water into the atmosphere again (the emergent flux).

The value of  $r_+$  is not affected by the interior of the water body and depends mainly on the angular composition of the incident light and the roughness of the water surface (wind speed). Values of  $A$  and especially  $R(z)$  are dependent on water IOPs, both being positively correlated with  $(b/a)$ .  $R(z)$  has been measured during several coccolithophore blooms, with maximum observed values in the top 20 m of 20% for PAR in the northeast Atlantic (Figure 7), 14% at 554 nm in the English Channel [*Garcia-Soto et al.*, 1995], 18% at 450 nm (estimated from coastal zone color scanner (CZCS)) off Brittany [*Viollier and Sturm*, 1984], 39% at 490 nm, and 33% at 550 nm in the Gulf of Maine [*Balch et al.*, 1991]. However, a large proportion (as much as 70 or 80%) of the upwelling photons hitting the underside of the sea surface are reflected back down again, and so the

influence of coccolithophore blooms on ocean albedo (on  $A$ ) is not as great as on  $R(z)$ . For the standard conditions ( $0.75 \text{ mg chl } a \text{ m}^{-3}$ ,  $\theta = 45^\circ$ ,  $5 \text{ m s}^{-1}$  wind speed, and 25% cloud cover) used here, the COPT model predicts that increasing the calcite concentration from 0 to 100 to  $300 \text{ mg CaCO}_3\text{-C m}^{-3}$  will increase  $A$  ( $\text{W m}^{-2}$ , PAR) from 6.9% to 8.4% to 11.7%, whereas HYDROLIGHT predicts  $A$  ( $\text{W m}^{-2}$ , PAR) increases from 5.0% to 6.5% to 9.9%. Coccolithophore blooms therefore cause a maximum of a twofold increase in the ocean albedo, for the chlorophyll, gilvin, and meteorological conditions assumed here. Modeling of the wind-blown water surface is a complex modeling problem [*Mobley*, 1994, chap. 4] and HYDROLIGHT contains a more sophisticated representation of the water surface than does COPT, and so its albedo calculations are therefore likely to be more accurate. The high-coccolith albedos cannot be directly compared to observational data, but measurements of ocean albedo under low-coccolith conditions [*Payne*, 1972] showed low albedos of 5–7% for partially overcast skies with  $\theta \simeq 45^\circ$  and wind speed  $\simeq 5 \text{ m s}^{-1}$ .

The results here can be used to make a rough estimate of the impact of coccolithophore blooms on global annually averaged albedo. If it is assumed that a typical coccolithophore bloom (one which can be detected by satellite) comes from water with  $100 \text{ mg CaCO}_3\text{-C m}^{-3}$  and  $0.75 \text{ mg chl } a \text{ m}^{-3}$ , then the increase in albedo due to this bloom needs to be multiplied by a global coverage in order to calculate a global impact. *Brown and Yoder* [1994], from analysis of a global data set of CZCS satellite images over several years, estimate an annual extent of coccolithophore blooms of  $\sim 1.4 \times 10^6 \text{ km}^2$  worldwide. If each bloom is assumed to persist for about 1 month, then the summed impact will be equal to

$$\begin{aligned} (6.5\% - 5.0\%) \times (1.4 \times 10^6 \text{ km}^2 \div 5.1 \times 10^8 \text{ km}^2) \times \left(\frac{1}{12}\right) \\ = 0.0003\% \end{aligned} \quad (10)$$

where  $5.1 \times 10^8 \text{ km}^2$  is the surface area of Earth. To this total should be added a contribution by blooms not included in the Brown and Yoder total, for instance, those which are too small in area or too short in duration. Persistent cloud cover in poorly sampled areas also possibly leads to underestimates of global bloom area. However, even a doubling of 0.0003% is still a negligible effect. This effect is small because, according to the CZCS analysis [*Brown and Yoder*, 1994], the blooms cover only a small fraction of the planet's area (0.3%) and that only for 1 month in each year.

A more important effect is likely to be that coming from subbloom or background concentrations of coccolithophores. Unpublished data from the Atlantic Meridional Transect (AMT) cruises (E. Marañón, personal communication, 1997) suggests an average calcite con-

centration in surface waters across the Atlantic oligotrophic gyres of  $\sim 10$  mg  $\text{CaCO}_3\text{-C m}^{-3}$ , with chlorophyll *a* concentrations averaging  $\sim 0.1$  mg chl *a m}^{-3}. To take the extreme case, it can be assumed that all the calcite is in the form of coccoliths and that this concentration of coccoliths holds for all oceans from  $60^\circ\text{S}$  to  $60^\circ\text{N}$  and for all months of the year. *Emiliania huxleyi* is known to be a cosmopolitan species, occurring in large numbers in all oceans except the polar ones [Winter et al., 1994]. Estimated flux of calcium carbonate from surface waters [Milliman, 1993, Figure 6] is approximately twofold to fourfold higher in subpolar latitudes than in the subtropical gyres but only falls to zero in polar waters. The HYDROLIGHT model predicts ocean albedos of 4.93% for  $0$  mg  $\text{CaCO}_3\text{-C m}^{-3}$  and 5.15% for  $10$  mg  $\text{CaCO}_3\text{-C m}^{-3}$ , with gilvin absorption and chlorophyll set to oligotrophic values of  $a_y(440) = 0.025$  and  $0.1$  mg chl *a m}^{-3}. Consequently an upper bound on the global albedo impact can be calculated as**

$$(5.15\% - 4.93\%) \times (3.1 \times 10^8 \text{ km}^2 \div 5.1 \times 10^8 \text{ km}^2) \times \left(\frac{12}{12}\right) \\ = 0.13\% \quad (11)$$

where  $3.1 \times 10^8 \text{ km}^2$  is an estimate of the area of the oceans between  $60^\circ\text{S}$  and  $60^\circ\text{N}$ .

These calculations, albeit uncertain, allow us to estimate that the total impact of coccolith light scattering on making the planet more reflective to sunlight is to increase the average planetary albedo by not more than 0.13%. An average of  $340 \text{ W m}^{-2}$  of solar radiation arrives at the top of the atmosphere, and of that approximately half penetrates to the planet's surface [Schneider, 1992]. The value of  $0.13\% \times 170 \text{ W m}^{-2}$  gives a maximum radiative forcing impact of  $0.22 \text{ W m}^{-2}$ . By comparison, the anthropogenic input of extra greenhouse gases into the atmosphere since the 1700s is estimated to have already caused an additional radiative forcing of  $\sim 2.5 \text{ W m}^{-2}$  [Shine et al., 1990], and  $\text{CO}_2$  doubling would change radiative forcing by  $\sim 4 \text{ W m}^{-2}$  [Kiehl, 1992].

## 7. Conclusions

A Monte Carlo model for simulating optics during coccolithophore blooms has been described. The validation of the model against other models and against optical data collected during a coccolithophore bloom is described. The model has then been used to analyze the precise effects of high coccolith concentrations on ocean optics, and these have been shown to include (1) increased brightness and heating of the water just beneath the surface, (2) increased albedo of the ocean due to photons reemerging from the water after having been scattered by coccoliths, (3) stronger stratification, (4) net cooling of the water column, and (5) decreased total water column productivity.

The albedo impact of coccolithophore blooms is shown to be unimportant in global climate terms because of the relatively small area covered. Light scattering due to subbloom coccolith concentrations has greater potential to influence global albedo and climate but is still a small forcing relative to that caused by greenhouse gases such as  $\text{CO}_2$ . Coccolithophore blooms may have greater climatic importance in other ways, for instance, through the effects of coccolith formation on  $\text{CO}_2$  [Holligan and Robertson, 1996].

**Acknowledgments.** We gratefully acknowledge the help of Barney Balch, Paul van der Wal, Runar Dalløkken, Gerald Moore, and Polly Machin in obtaining optical data. The paper has benefited from discussions with and comments from Cheng-Chien Liu, Jill Schwarz, Gerald Moore, Barney Balch, Steve Groom, Gavin Reeder, John Kirk, and Jim Aiken. T.T. and P.M.H. acknowledge support from the U.K. Natural Environment Research Council as part of the Plankton Reactivity in the Marine Environment (PRIME) program. C.D.M. acknowledges support from the Environmental Optics Program of the U.S. Office of Naval Research, which also supported in part the development of HYDROLIGHT. PRIME publication 45.

## References

- Ackleson, S.G., W.M. Balch, and P.M. Holligan, White waters of the Gulf of Maine, *Oceanography*, 1(2), 18–22, 1988.
- Ackleson, S.G., W.M., Balch, and P.M. Holligan, The response of water-leaving radiance to particulate calcite and pigment concentration: A model for Gulf of Maine coccolithophore blooms, *J. Geophys. Res.*, 99(C4), 7483–7499, 1994.
- Balch, W.M., P.M. Holligan, S.G. Ackleson, and K.J. Voss, Biological and optical properties of mesoscale coccolithophore blooms in the Gulf of Maine, *Limnol. Oceanogr.*, 36, 629–643, 1991.
- Balch, W.M., K.A. Kilpatrick, and C.C. Trees, The 1991 coccolithophore bloom in the central North Atlantic, 1, Optical properties and factors affecting their distribution, *Limnol. Oceanogr.*, 41, 1669–1683, 1996a.
- Balch, W.M., K.A. Kilpatrick, P.M. Holligan, D.S. Harbour, and E. Fernández, The 1991 coccolithophore bloom in the central North Atlantic, 2, Relating optics to coccolith concentration, *Limnol. Oceanogr.*, 41, 1684–1696, 1996b.
- Brown, C.W., and J.A. Yoder, Coccolithophorid blooms in the global ocean, *J. Geophys. Res.*, 99(C4), 7467–7482, 1994.
- Cox, C., and W. Munk, Measurements of the roughness of the sea surface from photographs of the sun's glitter, *J. Opt. Soc. Am.*, 44(11), 838–850, 1954.
- García-Soto, C., E. Fernández, R.D. Pingree, and D.S. Harbour, Evolution and structure of a shelf coccolithophore bloom in the Western English Channel, *J. Plankton Res.*, 17(11), 2011–2036, 1995.
- Gordon, H.R., and A. Morel, *Remote Assessment of Ocean Color for Interpretation of Satellite Visible Imagery: A Review*, *Coastal Estuarine Stud.*, vol. 4, Springer-Verlag, New York, 1983.
- Gordon, H.R., O.B. Brown, R.H. Evans, J.W. Brown, R.C. Smith, K.S. Baker, and D.K. Clark, A semianalytic radiance model of ocean color, *J. Geophys. Res.*, 93(D9), 10,909–10,924, 1988.

- Harrison, A.W., and C.A. Coombes, An opaque cloud cover model of sky short wavelength radiance, *Sol. Energy*, 41(4), 387-392, 1988.
- Holligan, P.M., and W.M. Balch, From the ocean to cells: Coccolithophore optics and biogeochemistry, in *Particle Analysis in Oceanography*, edited by S. Demers, NATO ASI Ser., Ser. G, 27, 1991.
- Holligan, P.M., and J.E. Robertson, Significance of ocean carbonate budgets for the global carbon cycle, *Global Change Biol.*, 2, 85-95, 1996.
- Holligan, P.M., M. Viollier, D.S. Harbour, P. Camus, and M. Champagne-Philippe, Satellite and ship studies of coccolithophore production along a continental shelf edge, *Nature*, 304, 339-342, 1983.
- Holligan, P.M., et al. A biogeochemical study of the coccolithophore *Emiliania huxleyi* in the North Atlantic, *Global Biogeochem. Cycles*, 7(4), 879-900, 1993.
- Kiehl, J.T., Atmospheric general circulation modeling, in *Climate Systems Modeling*, edited by K.E. Trenberth, pp. 319-369, Cambridge Univ. Press, New York, 1992.
- Kirk, J.T.O., Monte Carlo procedure for simulating the penetration of light into natural waters, *Tech. Pap. 36*, Commonwealth Sci. and Ind. Res. Org., Div. of Plant Ind, Melbourne, Australia, 1981.
- Kirk, J.T.O., *Light and Photosynthesis in Aquatic Ecosystems*, 2nd ed., Cambridge Univ. Press, New York, 1994.
- Mann, K.H., and J.R.N. Lazier, *Dynamics of Marine Ecosystems: Biological-Physical Interaction in the Oceans*, Blackwell Sci., Cambridge, Mass., 1991.
- Milliman, J.D., Production and accumulation of calcium carbonate in the ocean: Budget of a nonsteady state, *Global Biogeochem. Cycles*, 7(4), 927-957, 1993.
- Mobley, C.D., *Light and Water; Radiative Transfer in Natural Waters*, Academic, San Diego, Calif., 1994.
- Mobley, C.D., *HYDROLIGHT 3.0 User's Guide*, Proj. Rep. 5632, SRI Int., Menlo Park, Calif., 1995.
- Mobley, C.D., B. Gentili, H.R. Gordon, Z. Jin, G.W. Kattawar, A. Morel, P. Reinersman, K. Stamnes, and R.H. Stavn, Comparison of numerical models for computing underwater light fields, *Appl. Opt.*, 32(36), 7484-7504, 1993.
- Morel, A., and L. Prieur, Analysis of variations in ocean colour, *Limnol. Oceanogr.*, 22, 709-722, 1977.
- Nanninga, H.J., and T. Tyrrell, The importance of light for the formation of algal blooms by *Emiliania huxleyi*, *Mar. Ecol. Prog. Ser.*, 136, 195-203, 1996.
- Payne, R.E., Albedo of the sea surface, *J. Atmos. Sci.*, 29, 959-970, 1972.
- Plass, G., T. Humphreys, and G. Kattawar, Ocean-atmosphere interface: Its influence on radiation, *Appl. Opt.*, 20, 917-931, 1981.
- Roesler, C.S., M.J. Perry, and K.L. Carder, Modeling in-situ phytoplankton absorption from total absorption spectra in productive inland marine waters, *Limnol. Oceanogr.*, 34, 1510, 1989.
- Schneider, S.H., Introduction to climate modeling, in *Climate Systems Modeling*, edited by K.E. Trenberth, pp. 3-26, Cambridge Univ. Press, New York, 1992.
- Shine, K.P., R.G. Derwent, D.J. Wuebbles, and J.-J. Morcrette, Radiative forcing of climate, in *Climate Change: The IPCC Assessment*, edited by J.T. Houghton, G.J. Jenkins, and J.J. Ephraums, pp. 41-68, Cambridge Univ. Press, New York, 1990.
- Smith, R.C., and K.S. Baker, Optical properties of the clearest natural waters (200-800nm), *Appl. Opt.*, 20, 177-184, 1981.
- Stavn, R., R. Schiebe, and C. Gallegos, Optical controls on the radiant energy dynamics of the air/water interface. The average cosine and the absorption coefficient, in *Ocean Optics VII*, edited by M.A. Blizzard, *Proc. Soc. Photo-Opt. Instrum. Eng.*, 489, 62-67, 1984.
- Tyrrell, T., and A.H. Taylor, A modelling study of *Emiliania huxleyi* in the NE Atlantic, *J. Mar. Syst.*, 9(1/2), 83-112, 1996.
- Viollier, M., and B. Sturm, CZCS data analysis in turbid coastal waters, *J. Geophys. Res.*, 89, 4977-4985, 1984.
- Winter, A., R. Jordan, and P. Roth, Biogeography of living coccolithophores in ocean waters, in *Coccolithophores*, edited by A. Winter and W.G. Siesser, pp. 39-49, Cambridge Univ. Press, New York, 1994.

---

P. M. Holligan and T. Tyrrell, School of Ocean and Earth Science, Southampton Oceanography Centre, University of Southampton, European Way, Southampton, SO14 3ZH, United Kingdom. (t.tyrrell@soc.soton.ac.uk)

C. D. Mobley, Sequoia Scientific Inc., 9725 SE 36th Street, Suite 308, Mercer Island, WA 98040.

(Received September 11, 1998; revised October 21, 1998; accepted October 23, 1998.)